BAUET JOURNAL
Published by
Bangladesh Army University of Engineering & Technology (BAUET)
Journal Homepage: https://journal.bauet.ac.bd/
DOI: https://doi.org/10.59321/BAUETJ.V5I1.3

Mathematical Modeling for Nanofluid Simulation in Porous Media

Md. Rasel Rana Khandaker[1], Md. Jahirul Haque Munshi[2*], Md. Mahmud Alam[3], Md. Nasir Uddin[4]

[1]Department of Mathematics, Dhaka University of Engineering and Technology (DUET), Gazipur-1700, Bangladesh
[2]Department of Mathematics, Faculty of Science, Engineering and Technology Hamdard University Bangladesh, Hamdard Nagar, Gazaria, Munshigonj-1510, Bangladesh
[3]Department of Mathematics, Dhaka University of Engineering and Technology (DUET), Gazipur-1700, Bangladesh
[4]Department of Mathematics, Bangladesh Army University of Engineering & Technology (BAUET), Qadirabad Cantonment, Dayarampur, Natore-6431, Bangladesh

Abstract: The computational analysis of laminar mixed convection nanofluid flow has been conducted in a two-dimensional rhombus-shaped enclosure featuring a protective cover and a centrally heated cool obstacle. This study primarily focused on assessing the effects of copper nanoparticles dispersed in water as the base fluid, specifically addressing the topic of nanofluids. The temperature discrepancy produced on by the opposing motion of the enclosure's top and bottom walls the top wall being cold and the bottom wall being cold as well will be essentially propels this mixed convection. The opposing wall is heated, whereas the opposite wall is unheated. The study evaluates whether streamlines, isotherms, velocity profiles, dimensionless temperature, average Nusselt numbers, and average fluid temperature have been affected by the Richardson and Darcy numbers, among other variables. The results indicate that both the Richardson and Darcy numbers exhibit an important effect on the system's flow patterns and the distribution of temperatures. Furthermore, regulating heat transfer in fluid flow via the porous material inside an enclosure hinge entirely on the Darcy number. The study provides a heat transfer correlation for the average Nusselt number while also taking into consideration various Darcy & Richardson parameters.

Keywords: *Mixed Convection; Nanofluid; Porous Media; Finite element method; Heat transfer*

Introduction: Analyzing the influence of thermal radiation on the simultaneous conduction circulation of heat in a porous environment is crucial for space technology and high-temperature operations, and it has many essential applications. Additionally, fluid flow and heat transmission in porous materials have attracted a lot of attention over the past few decades. This is primarily due to the numerous applications of flow through porous media, such as filtration, separation processes in chemical manufacturing, geothermal extraction, groundwater pollution, transpiration cooling, and storage of radioactive nuclear waste, purification, aquifer transport processes, and fiber insulation.

Escalators, buildings with elevators, air conditioning systems, air conditioning and heating technologies, building climate administration, heat exchangers, solar collectors, as well as astrophysics and biology, represent only a few of the real-world applications regarding the results of the study. The thorough evaluations by Nield and Bejan [1] and Ingham and Pop [2] provide comprehensive clarifications on various application areas. Enhancing the transportation of heat in cavities has emerged as an important challenge for the power generation and industrial sectors. To improve heat transport within cavities, researchers have conducted out in-depth studies in recent years utilizing experimental, analytical, and computer science methods. The uses of nanofluids for enhanced heat transfer were the primary focus of one prominent study by Xuan and Li [3]. They discovered that these nanofluids have an immense number of possibilities in improving the heat transfer procedure via the addition of CuO nanoparticles to the starting point fluids. The development of fluids that are adept at economically supporting heat exchange is essential in order to fulfill the increasing needs of contemporary technology, particularly nuclear power generation, microelectronics, and chemical production. Nanofluids were a class of fluids that display promise in this respect. These heat-transfer fluids have been referred to as nanofluids because they have a tiny concentration of nanoparticles embedded within a base fluid. Incorporating nanoparticles to the base fluid, even at humble volume fractions (1–5%), can significantly boost the thermal conductivity by about 20%, as demonstrated by a large body of research [4], [5], and [6]. The influence of natural convection on heat and mass transmission in a curved triangular cavity has been investigated through Rahman et al. [7] in a related study. Furthermore, double-diffusive convection in an inclined porous enclosure with opposing temperature and concentration gradients has been researched by Chamkha and Naser [8]. Teamah [9] performed numerical simulations of double-diffusive convection that is natural flow in a rectangular box using the finite volume direction. Their investigation took into account how a heat source and magnetic field affected the flow. The computational modeling of transfer of heat in a wavy enclosure with and without fins has been examined by Al Mahmud et al. [10]. The simulation of nanofluid flow in porous square enclosures has been looked at by Munshi et al. [11]. A study on the mathematical modeling of airborne convection flow employing magneto-hydrodynamics in a semi-circular heater with an undulating upper enclosure was additionally carried out by

Article history:
Received: 10 June 2025
Received in revised form: 15 September 2025
Accepted: 10 November 2025
Available online: 15 December 2025

Corresponding author details: Dr. M. J. H. Munshi
E-mail address: jahir.buet.bd@gmail.com
Tel: +8801819274767

Islam et al. [12]. MHD mixed convection has been investigated by Oztop et al. [13] in a lid-driven cavity with a heater at one of the corners. In an identical work, Munshi et al. [14] investigated whether a nanofluid impacted the transportation of heat in a U-shaped enclosure that was constructed from porous material. Using nanofluids in a lid-driven squares container filled with a media that is porous, Munshi et al. [15] further investigated the numerical simulation of both convection and conduction heat transfer. Furthermore, hydrodynamic convection and conduction in a lid-driven square chamber with an elliptic-shaped heated block with a corner heater has been investigated by Munshi et al. [16]. A computational study has been carried out by Khandaker et al. [17] in order to examine the effects of nanofluid flow within a porous enclosure with a rhombus-shaped geometry. The interaction with a continually heated obstacle throughout the enclosure constituted the main focus of the experiment. Khandaker et al. [18] analyzed heat-generating obstacle of nanofluid flow in a rhombus shaped enclosure filled with porous medium. Maxwell-Garnett [19] employs metallic films and glasses to produce colures. The viscosity of concentrated suspensions and solutions was examined by H. C. Brinkman [20]. The finite element method has been investigated by Zienktewicz et al. [21].

The literature recently in publishing has given not enough attention to the issue of convection and conduction heat transfer problem in a lid-driven enclosure with several features. Thus, this study proposes the effect of nanofluid flow in a rhombus-shaped porous material on a continuous heated and cold obstacle in order to fill this research gap. This particular study's main goal is to model and examine the previously indicated circumstances.

Physical Configuration: The modeling of the flow of nanofluid in a rhombus-shaped container with heating boundaries and porous media is demonstrated in Fig. 1. The top and bottom lids containing the cold-temperature obstacle move from left to right and left to right, correspondingly. While the left wall remained unheated, the right wall has been heated. Additionally, the internal temperature of the building serves as a constant source of both heat and cold.

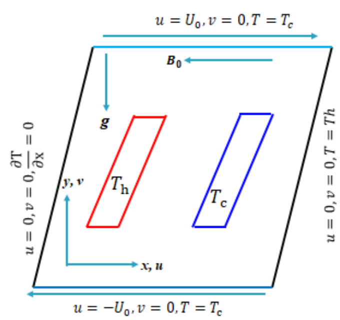

Fig. 1: Conceptual arrangements of the measurement system, boundary, as well as physical representation.

Mathematical Formulations: Following is a possible expression for the fundamental non-linear partial differential equations, which are:

$$\frac{\partial u'}{\partial x'} + \frac{\partial v'}{\partial y'} = 0$$

$$u'\frac{\partial u'}{\partial x'} + v'\frac{\partial u'}{\partial y'} = -\frac{1}{\rho_{nf}}\frac{\partial p'}{\partial x'} + \frac{\mu_{nf}}{\rho_{nf}}\nabla^2 u' - \frac{(\rho\beta)_{nf}}{\rho_{nf}k}u'$$

$$u'\frac{\partial v'}{\partial x'} + v'\frac{\partial v'}{\partial y'} = -\frac{1}{\rho_{nf}}\frac{\partial p'}{\partial y'} + \frac{\mu_{nf}}{\rho_{nf}}\nabla^2 v' - \frac{(\rho\beta)_{nf}}{\rho_{nf}k}v' + \frac{(\rho\beta)_{nf}}{\rho_{nf}k}g\beta(T - T_c) - \frac{\sigma_{nf}}{\rho_{nf}}{B_0}^2 v'$$

$$u'\frac{\partial T'}{\partial x'} + v'\frac{\partial T'}{\partial y'} = \alpha_{nf}\nabla^2 T'$$

The nanofluid properties expressed as:

$$\rho_{nf} = (1-\varphi)\rho_f + \varphi\rho_s$$

$$\alpha_{nf} = \frac{k_{nf}}{(\rho c_p)_{nf}}$$

$$(\rho C_p)_{nf} = (1-\varphi)(\rho C_p)_f + \varphi(\rho C_p)_s$$

$$(\rho\beta)_{nf} = (1-\varphi)(\rho\beta)_f + \varphi(\rho\beta)_s$$

$$\mu_{nf} = \frac{\mu_f}{(1-\varphi)^{2.5}}$$

$$k_{nf} = \frac{k_s + 2k_f - 2\varphi(k_f - k_s)}{k_s + 2k_f + \varphi(k_f - k_s)} \times k_f$$

The dimensional constraints on boundaries: No-slip boundary specifications regarding velocity ($u' = 0, v' = 0$) is used on every wall, with the exception of the top and bottom lids. On the top of the lid ($u' = U', v' = 0$) with cold temperature is applied, while on the bottom of the lid ($u' = -U', v' = 0$) with cold temperature is applied. The right wall is heating and left wall is adiabatic.

The next few dimensionless quantities are at present being implemented.

$$X' = \frac{x'}{L'}, Y' = \frac{y'}{L'}, U' = \frac{u'}{U'\alpha_f}, P' = \frac{p'}{\rho_{nf} U'^2}, \theta' = \frac{T' - T_c}{T_h - T_c}$$

The subsequent dimensionless equations that govern are generated by the replacement of the dimensional variable:

$$\frac{\partial U'}{\partial X'} + \frac{\partial V'}{\partial Y'} = 0$$

$$U'\frac{\partial U'}{\partial X'} + V'\frac{\partial U'}{\partial Y'} = -\frac{\partial P'}{\partial X'} + \frac{1}{Re}\frac{\mu_{nf}}{\rho_{nf,}\gamma_f}\frac{1}{(1-\varphi)^{2.5}}\nabla^2 U' - \frac{(\rho\beta)_{nf}}{\rho_{nf}}\frac{1}{ReDa}U'$$

$$U'\frac{\partial V'}{\partial X'} + V'\frac{\partial V'}{\partial Y'} = -\frac{\partial P'}{\partial Y'} + \frac{1}{Re}\frac{\mu_{nf}}{\rho_{nf,}\gamma_f}\frac{1}{(1-\varphi)^{2.5}}\nabla^2 V' - \frac{(\rho\beta)_{nf}}{\rho_{nf}\beta_f}\frac{1}{ReDa}V' + \frac{(\rho\beta)_{nf}}{\rho_{nf}\beta_f}Ri\theta' - \frac{Ha^2}{Re}V'$$

$$U'\frac{\partial \theta'}{\partial X'} + V'\frac{\partial \theta'}{\partial Y'} = \frac{\alpha_{nf}}{\alpha_f}\frac{1}{RePr}\nabla^2\theta'$$

Re,Pr,Ri,Da,Ha and Gr are Reynolds number, Prandtl number, Richardson number, Darcy number, Hartmann number and Grashof number respectively.

The dimensionless constraints on boundaries: No-slip boundary specifications regarding velocity ($U' = 0, V' = 0$) is used on every wall, with the exception of the top and bottom lids. On the top of the lid ($U' = 1, V' = 0$) with cold temperature ($\theta' = 0$) is applied, while on the bottom of the lid ($U' = -1, V' = 0$) with cold temperature ($\theta' = 0$) is applied. The right wall is heating ($\theta' = 1$) and left wall is adiabatic.

In this work, the fluid and heat transportation mechanisms are shown employing streamlines and isotherms. The formula for continuity expresses the stream of function (ψ') as:

$$\frac{\partial \psi'}{\partial Y'} = U', -\frac{\partial \psi'}{\partial X'} = V'$$

Isotherms (θ') according to the energy equation, they have been defined as:

$$\frac{\partial \theta'}{\partial Y'} = U'T' - \frac{\partial T'}{\partial X'}, \qquad -\frac{\partial \theta'}{\partial X'} = V'T' - \frac{\partial T'}{\partial Y'}$$

The average number of Nusselt

$$Nu_{ave} = -\frac{1}{L}\int_0^L \frac{\partial T'}{\partial N} ds$$

Where L is the heated wall's length. In process engineering design calculations, the mean Nusselt number can be performed for determining the velocity of heat transfer from the heated surface. The literal meaning of the regional Nusselt number that appears on the left wall provides

$$Nu_{local} = \frac{K_{nf}}{K_f}\frac{\partial \theta'}{\partial X'}\bigg|_{X'=0}$$

Nanofluid properties: Properties of thermo-physical of nanofluid (H_2O, Cu) for the capacitance of heat (4179, 385) Density (997.1, 8933), Thermal conductivity (0.613, 401), Thermal coefficient expansion $(2.1 \times 10^{-4},\ 1.6 \times 10^{-5})$ and dynamic viscosity (0.001003).

Numerical Technique: The Galerkin weighted residual finite-element examine is employed for transforming the nonlinear conditions regulating partial differential coefficients that has been the mass, momentum, and energy coefficients into a system of equations governing integrals. The Gauss quadrature methodology is employed for carrying perform the integration expected in each of these equations' components. By implementing boundary constraints, the consequences of nonlinear algebraic equations are adjusted. Newton's modified nonlinear equations into linear algebraic equations. Subsequently the linear equations have been resolved using the triangular factorization procedure.

Table 1: Grid sensitivity $Pr = 0.71, Ri = 1$ and $Ha = 50$.

Nodes	832	1114	1725	6743	24136
Elements	1601	2146	3328	12270	48468
Nu_{av}	8.64276	8.66746	8.67727	8.70372	8.70841
Time (s)	8	11	14	20	35

The mean of the Nusselt numbers across the grid is displayed within Table 1. The grid size of 6743 nodes and 12270 elements, as illustrated in the table, presented an acceptable arrangement for this particular numerical investigation.

Validation regarding the Program: Fig. 2 demonstrates a comparison between streamlines and equilibrium temperatures for the graphical approach. Their combined total is what makes very apparent that both parties are in complete agreement. A substantial amount of concurrence between the two outcomes can be determined from the statistical analysis. It is the present state of my numerical place of employment, whose will be reviewed briefly in this research paragraph. This program has been modified into a rhombus-shaped enclosure in media that is porous.

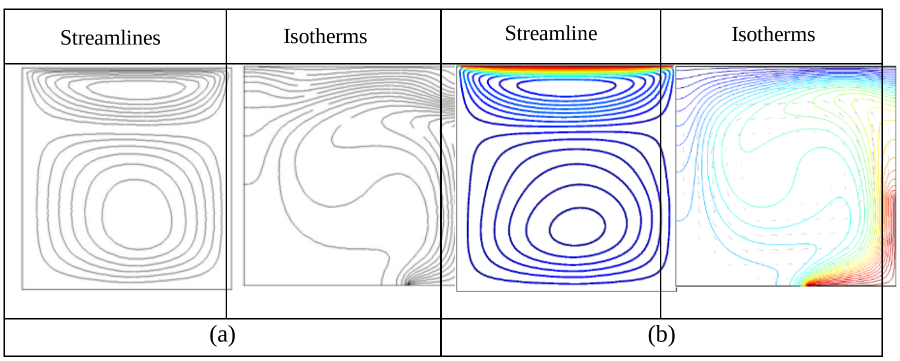

Fig. 2: Evaluation of streamlines and the isotherms for the computational solution of (a) Oztop et al. [13] (b) Latest study, Ra = 10^5, Re = 100, and Ha = 50.

Findings and discussion: The processes, fluid dynamics, and heat transfer discussed earlier have been obtained from the simulation software COMSOL Multiphysics. The original graphical outputs from COMSOL Multiphysics have been modified to present a more streamlined presentation, including isotherms, velocity profiles, local Nusselt numbers, and temperature measurements without dimensions. The Grashof number$(Gr = 10^4)$, Reynolds number $(Re = 100)$, Prandtl number $(Pr = 6.2)$, Hartmann number $(Ha = 50)$, and solid volume of the nanoparticle in a range of $\varphi = 5\%$ were all fixed during the computations. Fortunately the Darcy number (Da) fluctuates between $1e^{-5}\ to\ 1e^{-2}$and the Richardson number (Ri) fluctuates from 0.1 to 10. Experiments are carried out into the consequences of different arrangements of the constant heating cold obstacle.

Effect of Darcy number: With established parameters Ri = 1, Ha = 50, Pr = 6.2 and $\varphi = 5\%$, the streamline as well as isotherm movements under the consequences of a heated as well as cold obstruction are displayed in Fig. 3 and Fig. 4, correspondingly.

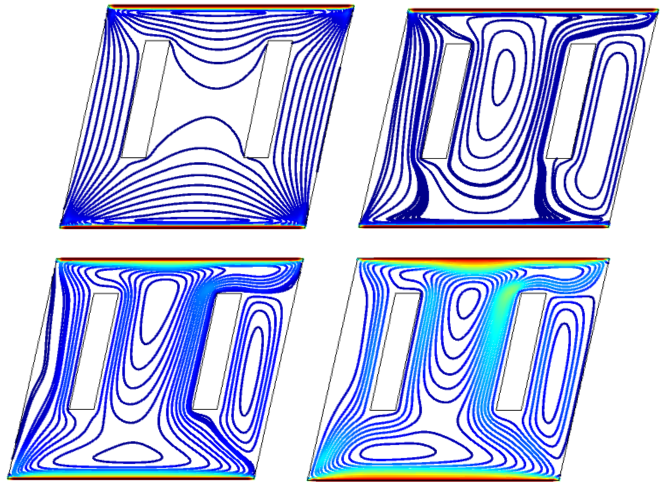

Fig. 3: Streamlines with different Darcy values of numbers $Da = 1e^{-5} - 1e^{-2}$ when $Ri = 1, Ha = 50, Pr = 6.2$ and $\varphi = 5\%$.

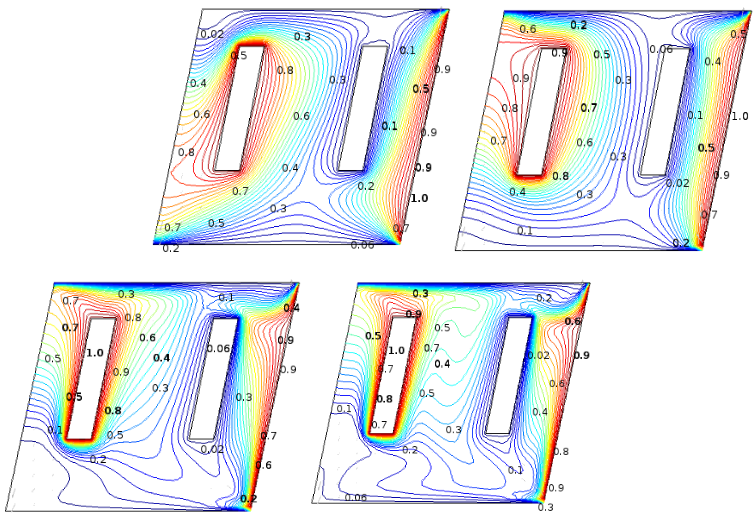

Fig. 4: Isotherms with different Darcy values of numbers $Da = 1e^{-5} - 1e^{-2}$ when $Ri = 1, Ha = 50, Pr = 6.2$ and $\varphi = 5\%$.

The Darcy number varies between $1e^{-5}$ to $1e^{-2}$. A substantial change in the swirling center carried on by the continuous heating obstruction can be observed in Fig. 3. Due to shear forces, a clockwise vortex forms within the object's body. Specifically, when the obstruction is placed in the central area of the enclosure, the counterclockwise spinning vortex flows partially toward the direction of movement of the taller wall. Furthermore, a counterclockwise rotating vortex gradually changes towards the center and rightmost walls whenever the number assigned to Darcy gets raised to $1e^{-2}$. Undoubtedly, the fluid flow underneath the continually heating barriers is significantly more intense than the region on the top, which is affected by the lid's motion. The isotherms of temperature in Fig. 4 demonstrate that conduction dominating heat transfer when Ri = 1, Ha = 50, Pr = 6.2 and $\varphi = 5\%$. Conduction-dominated transmission of heat is demonstrated by the equilibrium temperatures appearing parallel to the top wall at the lowest possible Darcy value. The isotherm lines become more twisted as Darcy increases. Especially along the left and right walls, demonstrating enhanced heat transfer through convection transport.

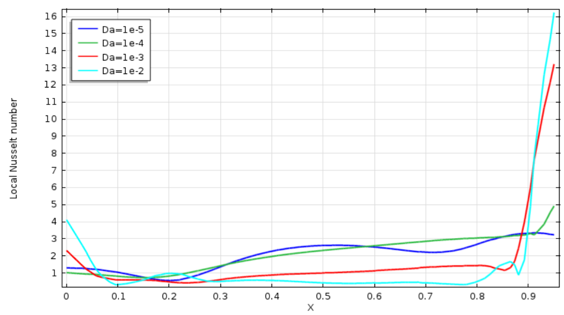

Fig. 5: Local Nusselt number variation along the enclosure's X-axis corresponding to different Darcy values for numbers $Da = 1e^{-5} - 1e^{-2}$ when $Ri = 1,\ Ha = 50, Pr = 6.2$ and $\varphi = 5\%$.

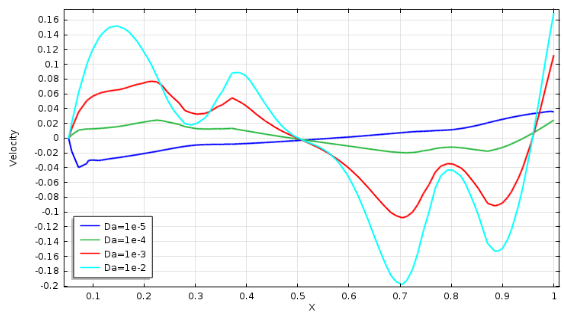

Fig. 6: Velocity profiles variation along the enclosure's X-axis corresponding to different Darcy values for numbers $Da = 1e^{-5} - 1e^{-2}$ when $Ri = 1,\ Ha = 50, Pr = 6.2$ and $\varphi = 5\%$.

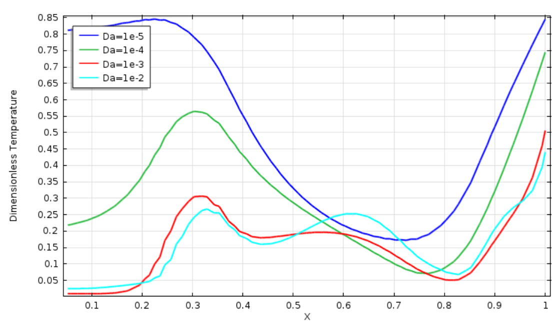

Fig. 7: Dimensionless temperature variation along the enclosure's X-axis corresponding to different Darcy values for numbers $Da = 1e^{-5} - 1e^{-2}$ when $Ri = 1,\ Ha = 50, Pr = 6.2$ and $\varphi = 5\%$.

Fig. 5 exhibits the local number of Nusselt along the X-axis based on different Darcy numbers having $Ri = 1, Ha = 50, Pr = 6.2$ and $\varphi = 5\%$ of the enclosures. The local number of Nusselt is uniform when compared to the enclosure's corresponding vertical line in recognition of the symmetry in the heating boundary circumstances. The figure demonstrates that in almost every instance of the perpendicular wall, the Nusselt number that is local increases as the number given by Darcy increases. In this particular instance, the local number for Nusselt increases more gradually as the Darcy number approaches. Fig. 6 illustrates changes of the velocity vertical component corresponding to the Darcy numbers along the enclosure's horizontal the center of the body As the number Darcy increases, the figure demonstrates that the absolute magnitudes of the maximum and minimum velocity numbers increase additionally. Maximum shaped curves are found for X < 0.5, whereas minimum constitute curves are found for X > 0.5, when X = 0.7 velocity profiles are the same as zero. The temperature profiles for various Darcy numbers along the bottom wall are displayed in Fig. 7. Both the highest and lowest temperatures are shown in this figure. The structure in the very center enables the intersecting lines to extend upwards.

Effect of Richardson Numbers: In numerical computations, the Richardson number increases throughout the laminar range Ri = 0.1-10, whereas the Darcy, Hartmann, and Prandtl numbers remain constant. Fig. 8 and Fig. 9 demonstrate modifications in streamlines and equilibrium temperatures whereas constant both hot and cold obstructions appear for different values of Ri = 0.1-10. There are two eddies in the enclosed space because both the hot and cold obstacles are separated from within it and their buoyancies are combined. Another time, the clockwise rotating vortex filtered the left and bottom right sidewalls little by little as the Richardson number approached. The fluid flow beneath the constant source and sink obstacle is obviously much lower than that of the highest point, which has been affected by the motion moving the lid. The isotherms in Fig. 9 demonstrate that conduction dominating the transmission of heat when Ri = 0.1-10. For the lowest possible amount of Ri, the isotherms appears parallel to the top wall, as demonstrated in the illustration. The isotherm lines are more bending on the left and right walls, showing increased heat transfer through convection transportation.

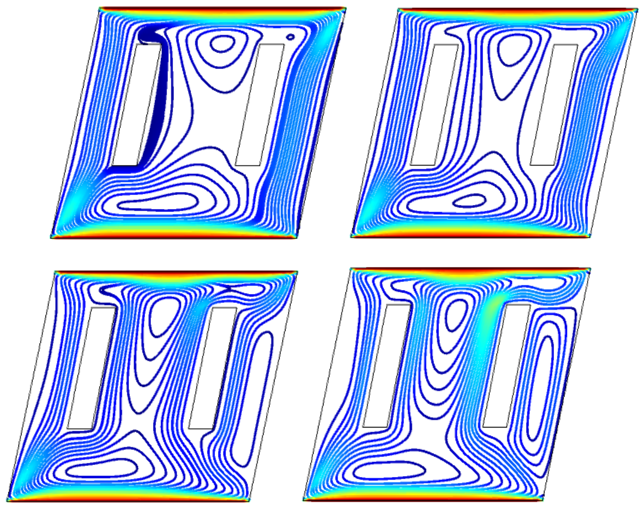

Fig. 8: Streamlines for different Richardson values for numbers $Ri = 0.1, 1, 5, 10$ when $Da = 1e^{-5}, Ha = 50, Pr = 6.2$ and $\varphi = 5\%$.

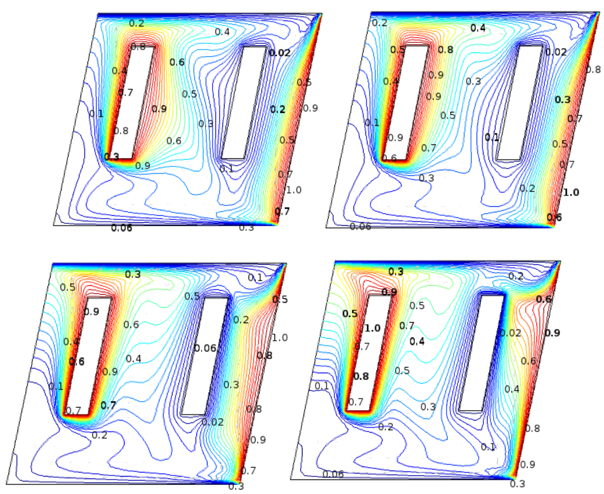

Fig. 9: Isotherms for different Richardson values for numbers $Ri = 0.1, 1, 5, 10$ when $Da = 1e^{-5}, Ha = 50, Pr = 6.2$ and $\varphi = 5\%$.

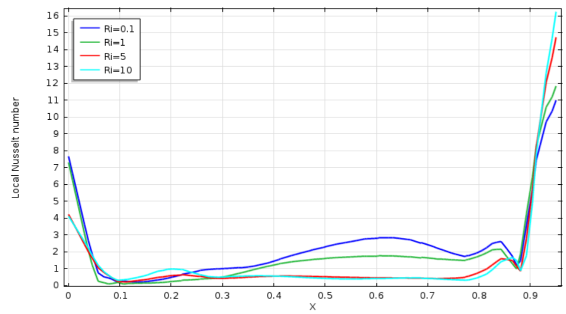

Fig. 10: Modifications in the local number of Nusselt throughout the enclosure's X-axis according to different Richardson numbers $Ri = 0.1, 1, 5, 10$ when $Da = 1e^{-5}, Ha = 50, Pr = 6.2$ and $\varphi = 5\%$.

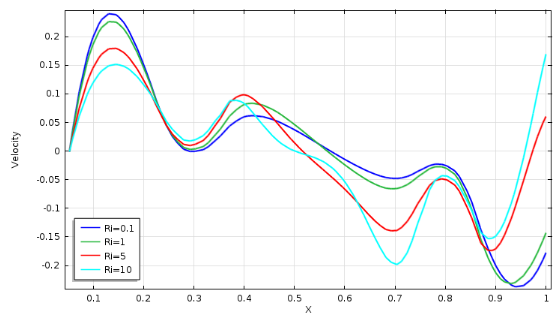

Fig. 11: Modifications in the velocity profile throughout the enclosure's X-axis according to different Richardson numbers $Ri = 0.1, 1, 5, 10$ when $Da = 1e^{-5}, Ha = 50, Pr = 6.2$ and $\varphi = 5\%$.

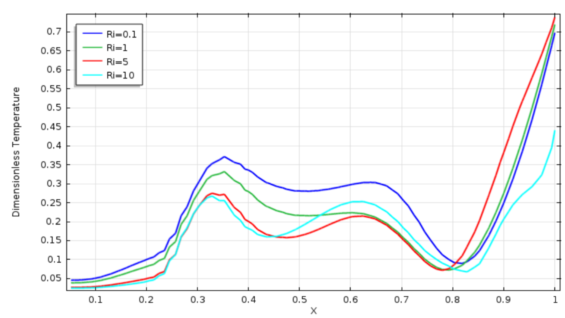

Fig. 12: Modifications in the dimensionless temperature throughout the enclosure's X-axis according to different Richardson number $Ri = 0.1, 1, 5, 10$ when $Da = 1e^{-5}, Ha = 50, Pr = 6.2$ and $\ddot{o} = 5\%$.

In Fig. 10, the local number of Nusselt along the X-axis appears for the different Richardson numbers $Ri = 0.1, 1, 5, 10$ when $Da = 1e^{-5}, Ha = 50, Pr = 6.2$ and $\varphi = 5\%$ of the enclosure. Parallel to the x-axis, a lower Richardson number local number of Nusselt value represents a more minor change; although a higher Richardson number local Nusselt number value represents less significant change. Fig. 11 demonstrates the variation of the profile of velocity along the X-axis according to different Richardson numbers $Ri = 0.1, 1, 5, 10$ when $Da = 1e^{-5}, Ha = 50, Pr = 6.2$ and $\varphi = 5\%$ of the enclosure. The visualization demonstrates that as the Richardson number decreases and the absolute magnitudes of the maximum and minimum velocity values simultaneously decrease. When $Da = 1e^{-5}, Ha = 50, Pr = 6.2$ and $\varphi = 5\%$, Fig. 12 demonstrates the temperature distributions along the bottom wall according to different Richardson numbers, $Ri = 0.1, 1, 5, 10$. This figure illustrates the smallest value, maximum, and temperature. When considering that both the warm and cold obstructions have been placed in the middle, the lines are directed downward.

Conclusion: The numerical outcomes have been provided for mixed convection flow patterns implementing nanofluid in a porous the enclosure. For numerous significant dimensionless groups, particularly Richardson number and the number of Darcy, outcomes have been achieved. The flow and temperature gradients throughout the enclosure have been significantly affected by both Darcy and the moving lid ordinations. Features of heat transfer and fluid movement within the enclosure were highly dependent on the heated obstacle. Lower heater length values, as measured according to the Darcy number, result in an increased average number calculated by Nusselt at the heated wall and lower average temperatures of the fluid in the enclosures. The flow and the temperature fields, in addition to the average number of Nusselt results, have been greatly affected by the heated an obstruction. Whenever a liquid moves through a material with porous enclosure, using Richardson number is a significant control parameter for the transfer of heat.

Acknowledgments: COMSOL Multiphysics is responsible for the simulation, and we acknowledge its significant contribution to the analysis and creating of the results presented in this work.

Conflicts of Interest: The author has no competing interests.

References:

[1] D.A. Nield, and A. Bejan, Convection in Porous Media, fourth ed., Springer, New York, 1999.
[2] D.B. Ingham, and I. Pop, Transport Phenomena in Porous Media, Pergamum, 1998.
[3] Y. Xuan, and Q. Li, Heat transfer enhancement of nanofluids, Int. J. Heat Fluid Flow, Vol. 21, 2000, pp. 58-64.
[4] K. Khanafer, K. Vafai, and M. Lightstone, Buoyancy-driven heat transfer enhancement in a two dimensional enclosure utilizing nanofluids, Int. J. Heat Mass Trans. 46, 2003, 3639-3653.
[5] A. Abu-Nada, Z. Masoud, and A. Hijazi, Natural convection heat transfer enhancement in horizontal concentric annuli using nanofluids, Int. Commn. Heat Mass Trans. 35, 2008, 657-665.
[6] S.E. Ahmed, A.M. Rashad, and R.S.R. Goria, Natural convection in triangular enclosures filled with nanofluid saturated porous media, J. Thermo. Heat Trans., 27, 2013, 700-706.
[7] M.M. Rahman, H.F. Oztop, and A. Ahsan, J. Orfi, Natural convection effects on heat and mass transfer in a curvilinear triangular cavity, Int. J. Heat Mass Trans. 55, 2012, 6250-6259.
[8] AJ. Chamkha, and H.A. Naser, Double-diffusive convection in an inclined porous enclosure with opposing temperature and concentration gradients, Int. J. Therm. Sci. 40, 2001, 227-244.
[9] M.A. Teamah, Numerical Simulation of double diffusive natural convection in rectangular enclosure in the presences of magnetic field and heat source, Int. J. Therm. Sci. 47, 2008, 237-248.
[10] M.A. Al Mahmud, M. J. H. Munshi, M. S. Islam, M. J. Islam, M. A. Mannan, M. M. Hasan, Numerical simulation of heat transfer in a wavy enclosure with and without the presence of fins, Asian Research Journal of Mathematics, 19(9) 2023, 95-104.
[11] M.J.H. Munshi, M.S. Islam, M.R.R. Khandaker, M.S. Hossain, Simulation of Nanofluid Flow in Porous Square-Shaped Enclosures, Journal of Scientific Research (JSR), 15(2) 2023, 383-399.
[12] M.M. Islam, M.A. Alim, M.M. Alam, M.J.H. Munshi, Simulation of Natural Convection Flow with Magneto-Hydrodynamics in a Wavy Top Enclosure with a Semi-Circular Heater, Open Journal of Applied Sciences (Scientific Research Publishing), 13, 2023, 591- 603.
[13] H.F. Oztop, K. Al-Salem, and I. Pop, MHD mixed convection in a lid-driven cavity with corner heater, International Journal of Heat and Mass Transfer, 54, 2011, 3494-3504.
[14] M.J.H. Munshi, R. C. Gope, M. S. Islam, M. M. Azad, Heat Transfer of Nanofluid in a Porous Medium U-shaped enclosure: Numerical Investigation, Jilin Daxue Xuebao (Gongxueban), Journal of Jilin University, 42(04) 2023, 535-548.
[15] M.J.H. Munshi, M.A. Alim, A.H. Bhuiyan and K.F.U. Ahmed, Numerical simulation of mixed convection heat transfers of nanofluid in a lid-driven porous medium square enclosure, AIP Conf.
Procedia Engineering, 2121, 2019, 030005- (1-9).
[16] M.J.H. Munshi, M.A. Alim, A.H. Bhuiyan and M. Ali, Hydrodynamic mixed convection in a lid-drivensquare cavity including elliptic shape heated block with corner heater, Published by Elsevier, Procedia Engineering, 194, 2017, 442- 449.
[17] M.R.R. Khandaker, M.J.H. Munshi, M. M. Alam, M.J. Islam, M.A.A. Mahmud, M.S. Islam, The Impact of Nanofluid Flow in a Rhombus-Shaped Porous Enclosure on a Constant Heated Obstacle, European Journal of Mathematics and Statistics, 4(6) 2023, 1-12.
[18] M.R.R. Khandaker, M.J.H. Munshi, M.M. Alam, Heat-generating Obstacle of Nanofluid Flow in a Rhombus shaped Enclosure Filled with Porous Media, International Journal of Fluid Mechanics & Thermal Sciences, 11(3) 2025, 50-61.
[19] Maxwell- Garnett, Colures in metal glasses and in metallic films, Philosophical Transaction of the Royal Society of London. Series A, Containing Papers of a Mathematical or Physical Character, 203, 1904, 385-420.
[20] H.C. Brinkman, The viscocity of concentrated suspensions and solutions, J. Chem. Phys., 20, 1952, 571-581.
[21] O.C. Zienktewicz, and R.L. Taylor, The finite element method, Fourth Ed., McGraw-Hill, 1991.